Fermi National Accelerator Laboratory

FERMILAB-FN-684

Short-Bunch Production and Microwave Instability Near Transition

K.Y. Ng and J. Norem

Fermi National Accelerator Laboratory
P.O. Box 500, Batavia, Illinois 60510

October 1999

Operated by Universities Research Association Inc. under Contract No. DE-AC02-76CH03000 with the United States Department of Energy

Disclaimer

This report was prepared as an account of work sponsored by an agency of the United States Government. Neither the United States Government nor any agency thereof, nor any of their employees, makes any warranty, expressed or implied, or assumes any legal liability or responsibility for the accuracy, completeness, or usefulness of any information, apparatus, product, or process disclosed, or represents that its use would not infringe privately owned rights. Reference herein to any specific commercial product, process, or service by trade name, trademark, manufacturer, or otherwise, does not necessarily constitute or imply its endorsement, recommendation, or favoring by the United States Government or any agency thereof. The views and opinions of authors expressed herein do not necessarily state or reflect those of the United States Government or any agency thereof.

Distribution

Approved for public release; further dissemination unlimited.

Copyright Notification

This manuscript has been authored by Universities Research Association, Inc. under contract No. DE-AC02-76CH03000 with the U.S. Department of Energy. The United States Government and the publisher, by accepting the article for publication, acknowledges that the United States Government retains a nonexclusive, paid-up, irrevocable, worldwide license to publish or reproduce the published form of this manuscript, or allow others to do so, for United States Government Purposes.

Short-Bunch Production and Microwave Instability Near Transition

K.Y. Ng[1] and J. Norem[2]

[1] *Fermi National Accelerator Laboratory,*[3] *P.O. Box 500, Batavia, IL 60510*
[2] *HEP Division, Argonne National Laboratory, Argonne, IL 60439*

Abstract. Some methods of making short bunches are reviewed. The experiment performed at the Brookhaven AGS for bunching near transition is reported. Microwave instability for coasting beam and bunched beam near transition is discussed and simulations are presented.

I INTRODUCTION

For the proton driver of the muon collider, bunching of intense proton bunches to rms length $\sigma_\tau \leq 2$ ns at extraction is desirable. There are two primary reasons. First, the proton bunch length is the only piece of information transmitted to the pions produced in the target and muons resulting in the decay of the pions. The shorter the length of the proton bunches, the less cooling of the muons will be necessary. Second, it will be easier to separate the muons polarized in the two helicities. The shorter the proton bunch length will result in higher muon polarization. The following are some ways to achieve narrow bunches using rf gymnastics:

(1) Lowering and increasing rf voltage

The rf is reduced adiabatically until the bunch spreads out and fills the bucket. The rf voltage is raised again suddenly. In a quarter synchrotron oscillation, a narrow bunch is obtained. The adiabatic process may take very long in order to allow the bunch to follow the change in the bucket. However, for a high-intensity bunch to stay at low momentum spread for a long time, it is likely that the microwave instability will develop. In order to avoid instability, we can snap the rf voltage down suddenly so that the rf bucket changes from Fig. 1(a) to 1(b). The bunch will be lengthened after a quarter synchrotron oscillation. The rf voltage is then snapped up again as in Fig. 1(c) and finally the lengthened bunch rotates into a narrow bunch. Of course, the rf nonlinearity will show up during bunch rotations. A second or third-order harmonic cavity will help in cancelling the rf nonlinearity. In practice, this method can shorten the bunch by a factor of at most 3 to 4.

(2) Debunching at unstable fixed point

The rf phase is suddenly shifted by 180° so that the bunch originally centered at the stable fixed point in Fig. 2(a) finds itself centered at the unstable fixed point in Fig. 2(b). The bunch will therefore spread out along the separatrices. After a while, the rf phase is shifted back by 180° as in Fig. 2(c). Synchrotron oscillation between $\frac{1}{4}$ and $\frac{1}{2}$ period will rotate the bunch into a narrow one. Again nonlinearity of the rf will show up in the bunch shape and a higher-order harmonic cavity will

[3] Operated by the Universities Research Association, Inc., under contract with the U.S. Department of Energy.

© 1995 American Institute of Physics

help. Also, this process may be slow because movement along the separatrices is slow. In practice, this method can shorten the bunch by a factor of at most 3 to 4.

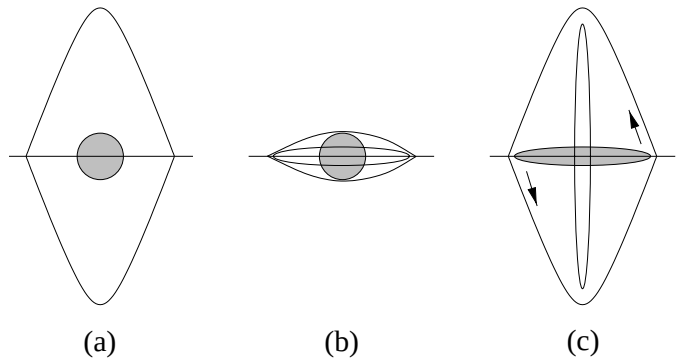

FIGURE 1. Bunch shortening is performed by snapping down the rf voltage $V_{\rm rf}$, rotating for $\frac{1}{4}$ synchrotron oscillation, snapping up $V_{\rm rf}$, and rotating for another $\frac{1}{4}$ synchrotron oscillation.

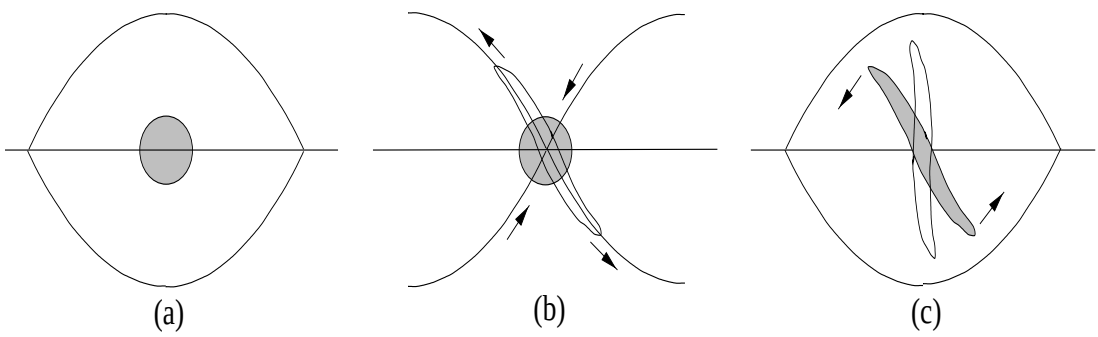

FIGURE 2. Bunch shortening is performed by shifting the rf phase by 180°, allowing the bunch to spread along the separatrices, shifting the rf phase by −180°, and rotating for $\frac{1}{4}$ to $\frac{1}{2}$ synchrotron oscillation.

(3) Rebunching at higher frequency

During the end of the ramping, the frequency of the rf system is jumped to the next higher multiple of the circulating frequency. This process continues and the bunch will gradually be shortened by following the change in width of the bucket. In practice, the rf frequency of a rf system cannot be changed by very much. Therefore, there must be several rf systems with frequencies one above the other, so that the lower-frequency system will be replaced by the next higher one, etc. Thus, this method involve several high-frequency and high-voltage rf systems and will be expensive. Also the whole procedure will be slow.

(4) Bunch-shortening near transition

At or near transition, there is little or no phase motion of the bunch particles. Thus, the particles continue to gain or lose energy according to the rf voltage they see, as is illustrated in Fig. 3(a), where the phase axis represents the rf phase of the particle when crossing the rf cavity gap. The bunch will shear in the momentum spread direction. A partial rotation will produce a narrow bunch, as depicted in Fig. 3(b). It is desirable to make the final bunching as fast as possible because of the large instantaneous currents produced in the ring, which can drive a variety

of instabilities. The final bunching can be made quite fast if the transition energy can be moved farther away from the beam energy and/or the rf voltage can be raised during the final rotation, thus raising the synchrotron frequency just before extraction. One of the merits of this method is that no additional hardware, such as higher-harmonic cavities, is required. Also this method uses only the linear part of the rf wave and a small synchrotron phase rotation. Thus the rotation can be made quite linear. We do not need to operate the ring at or near transition all the time. With the flexible momentum-compaction (FMC) lattice, the transition gamma can be varied to a large extent by varying the gradients of a pair of quadrupoles [1]. An example is shown in Fig. 4, where each of the two F-quadrupoles at a distance about $\frac{1}{3}$ from the entrance and exit of the FMC module has been split into a pair denoted by QFS and QF2. By varying the gradients of the QFS and QF2, the large variation of transition gamma is shown in the left plot of Fig. 5, and the corresponding values of the momentum-compaction factor α are listed on the right. The betatron tunes have been kept nearly unchanged during the variation. As a

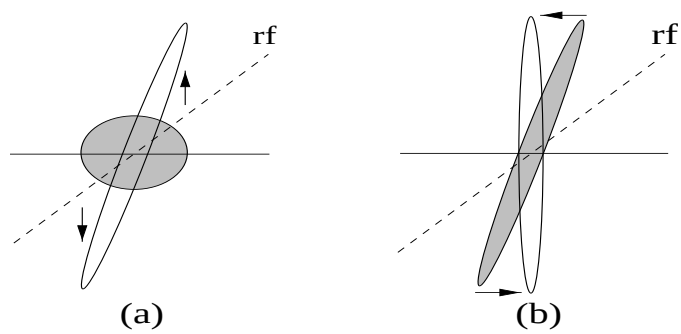

FIGURE 3. Bunch shortening is performed by allowing the bunch to shear very near to transition in the momentum direction, raising the rf, and rotating for $< \frac{1}{4}$ synchrotron oscillation.

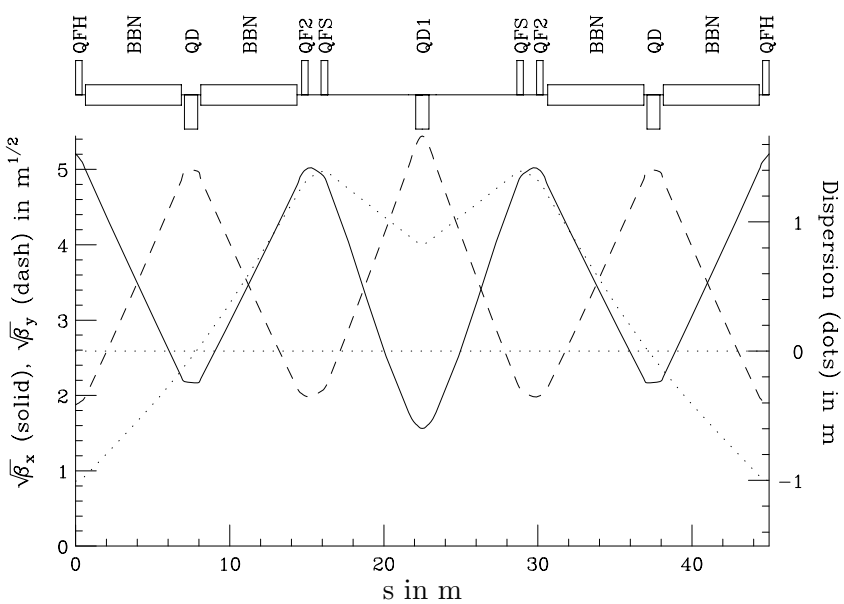

FIGURE 4. Two identical pairs of F-quadrupoles QFS and QF2 are installed at about $\frac{1}{3}$ from the entrance and exit of the FMC module. γ_t can be varied by varying their gradients.

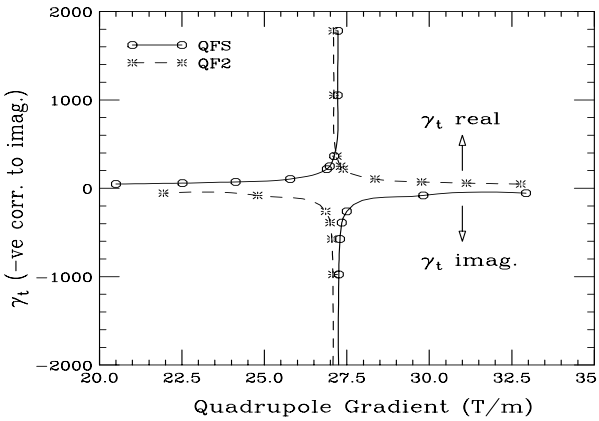

QFS (T/m)	QF2 (T/m)	α
12.89	38.60	+0.000424
17.23	35.56	+0.000191
19.52	33.56	+0.000021
20.29	32.77	+0.000001
27.23	27.08	−0.000000
27.28	27.04	−0.000003
27.50	26.85	−0.000015
32.93	21.93	−0.000335

FIGURE 5. When the gradients of the quadrupole pairs are varied, the transition gamma (left) and the corresponding momentum-compaction factor α (right) change by a wide range.

result, we can move close to or right at transition only at the moment when we want to make short bunches.

II EXPERIMENT ON BUNCH-SHORTENING NEAR TRANSITION

An experiment was performed at the Brookhaven AGS to demonstrate bunch-shortening near transition [2]. The operating mode of the AGS is shown in the left plot of Fig. 6. The maximum beam energy was reduced by flat-topping at 7 GeV, which shortened the acceleration period. The γ_t-jump system was modified to give a short flat-top period before the transition energy dropped. The beam was flat-

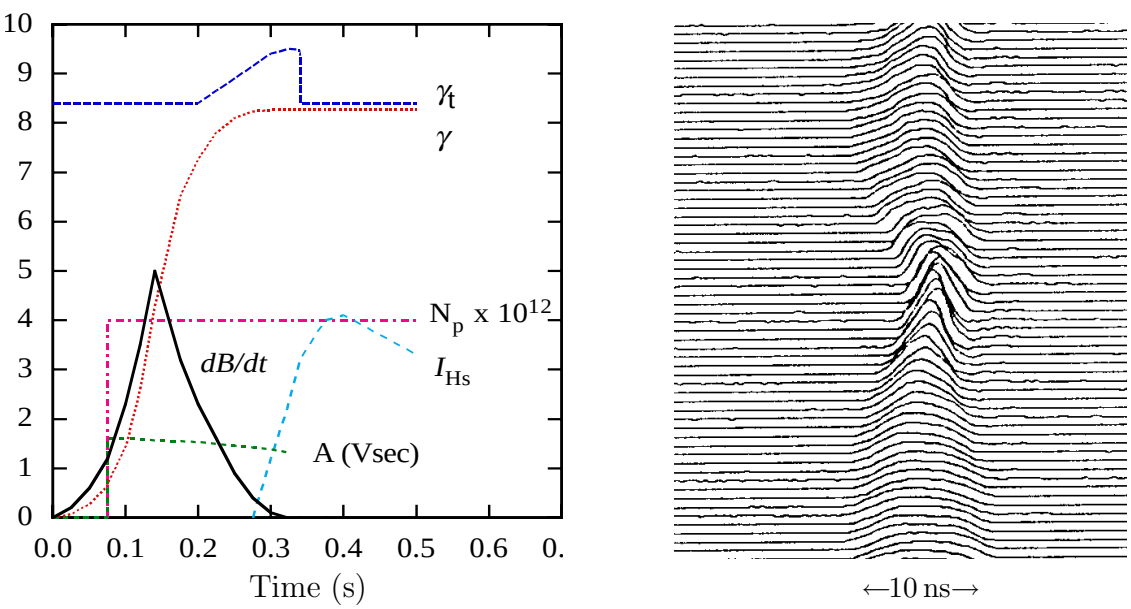

FIGURE 6. Left: The operating mode of the AGS, showing the magnet ramp dB/dt in 10^{-1} T/s, beam gamma γ, transition gamma γ_t, sextupole current I_{Hs} in 10 A, and longitudinal bunch area A in eV-s. Right: Mountain range plots of the bunch for about 50 ms starting 10 ms before the transition energy was dropped to near the beam energy.

topped for 300 ms before the magnet guide field was raised slightly and then ramped down. Only one bunch was injected, which has a bunch area of 1.5 ± 0.05 eV-s and an intensity of 3 to 5×10^{12} protons.

Because of the AGS γ_t-jump mechanism, the energy of the beam was kept at more than one unit of γ below γ_t. At about 0.35 s after injection, γ_t was dropped so that the beam was close to transition, with $|\gamma_t - \gamma| < 0.05$. The beam started to shear and at the same time rotate slowly. Here, no special hardware was available to move the beam away from transition and no other higher rf voltage was provided to perform the final partial rotation depicted in Fig. 3(b). For this reason, the beam cannot be too close to γ_t, otherwise the partial rotation will take very long. Likewise, it cannot be too far from γ_t, otherwise the bunch will shear not only in the momentum direction as required in Fig. 3(a), but also in the phase direction, so that a tall and narrow beam will not be produced. During this run, a new measurement of $\gamma_t = 8.34 \pm 0.05$ was made, which was best determined by measuring the synchrotron frequency.

A sample result is shown in the right plot of Fig. 6, which consists of mountain-range plots of the peak beam current and instantaneous current versus the machine phase sampled by the wall-gap monitor from 10 ms before the γ_t dropped to 40 ms after. We can see obviously that the bunch became narrow after the transition energy was dropped to near the beam energy.

The beam current versus time during the final bunch rotation is shown in the left plot of Fig. 7. The bunch shape corresponding to the situation when it is shortest was shown in the right plot of Fig. 7, together with its shape before the transition energy was lowered. The shortest rms bunch length recorded was $\sigma_\tau = 2.0$ ns and had been reduced 4 times.

Some important comments follow:
(1) During the whole experiment, no collective beam instability has been observed. However, the intensity has been 5 to 8 times below the required intensity of the 2.5×10^{13} bunch for the proton driver of the muon collider. The proton driver ramps a batch of 4 such bunches at the cycling rate of 15 Hz. It is unclear whether collective instability will occur or not at such a high intensity.

(2) The slip factor η is a function of momentum spread δ:

$$\eta(\delta) = \eta_0 + \eta_1 \delta + \mathcal{O}(\delta^2) \ , \tag{2.1}$$

where

$$\eta_0 = \frac{1}{\gamma_t^2} - \frac{1}{\gamma^2} \qquad \text{and} \qquad \eta_1 = \frac{1}{\gamma^2}\left[\alpha_1 + \frac{3\beta^2}{2}\right] + \eta_0 \left[\alpha_1 - \frac{1}{\gamma^2}\right] \ . \tag{2.2}$$

In above, $\alpha_0 = \gamma_t^{-2}$ is the lowest-order momentum-compaction factor and α_1 is the next higher order. They are defined as

$$C(\delta) = C_0 \left\{1 + \alpha_0 \delta \left[1 + \alpha_1 \delta + \mathcal{O}(\delta^2)\right]\right\} \ , \tag{2.3}$$

with C_0 being the length of the closed orbit for the on-momentum particle and

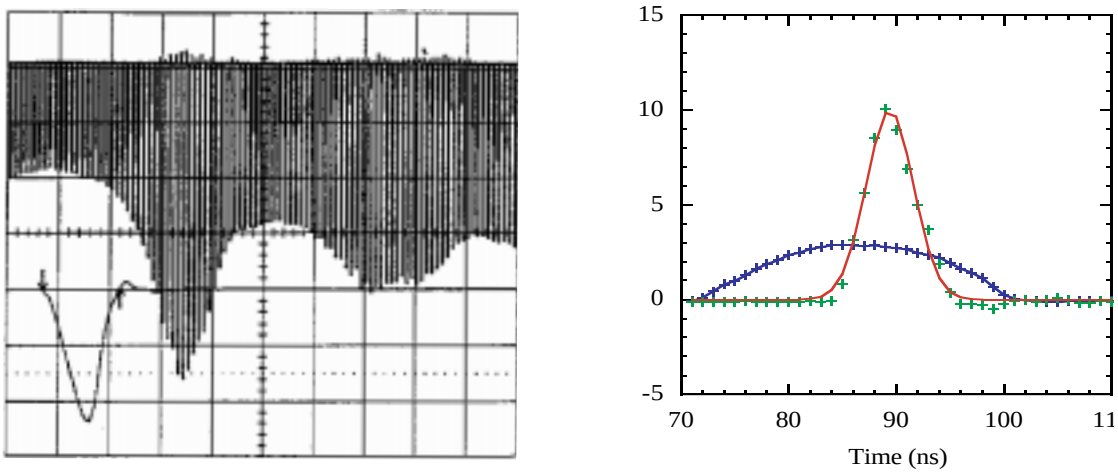

FIGURE 7. Left: Beam peak current versus time after γ_t was dropped. The bunch was seen executing synchrotron oscillations slowly giving a maximum peak current as a result of the shearing in momentum. The bunch shape at its narrowest instant is shown at the corner. Right: Bunch shapes before and after bunching near transition, showing a final narrow 1.5 eV-s bunch in crosses of rms width $\sigma_\tau = 2.0$ ns together with the best fitted Gaussian in solid.

$C(\delta)$ the closed orbit length at fractional momentum spread δ. Thus, even when $\gamma = \gamma_t$, η is linear in δ and the time-slip ΔT per revolution period T_0, given by

$$\frac{\Delta T}{T_0} = \eta\delta = \eta_0\delta + \eta_1\delta^2 + \mathcal{O}(\delta^3) \ , \tag{2.4}$$

becomes quadratic in δ. The drift in longitudinal phase will also be quadratic in δ. Therefore, instead of shearing linearly in the momentum direction as illustrated in Fig. 3(a), the bunch will shear nonlinearly as in left plot of Fig. 8. The result is that the final bunch will be wider. This nonlinear phase-slip can be corrected, for example, by deploying sextupoles. It is clear that when $\alpha_1 = -\frac{3}{2}$ and $|\eta_0| \ll 1$, the first-order nonlinear drift will be eliminated.

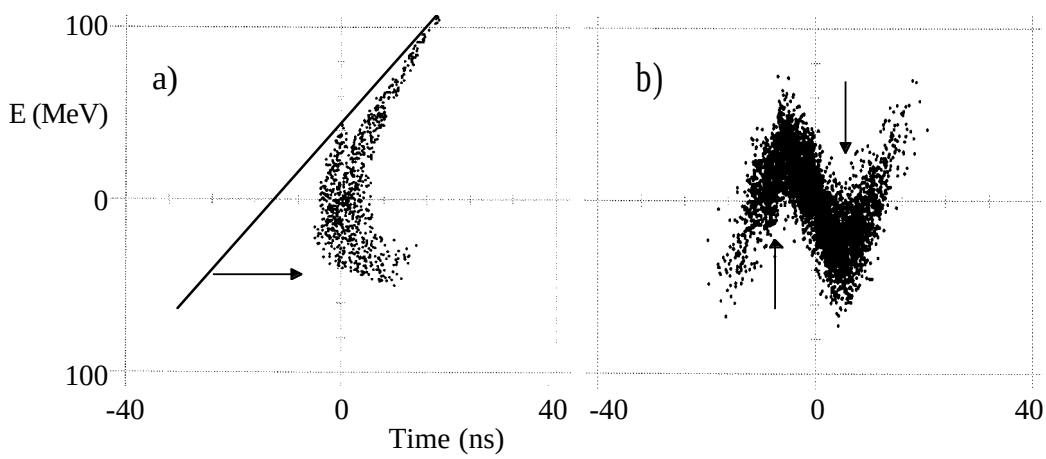

FIGURE 8. Effects of nonlinear η and space charge on the final phase space distribution. Left plot shows the effect of a quadratic horizontal shear which occurs when $\alpha_1 \neq -3/2$. Right plot shows the effect of vertical shear from strong space-charge effects.

(3) For an intense proton beam, space-charge effect cannot be ignored. The wake potential is essentially proportional to the slope of the bunch linear distribution. Thus, staying near transition for too long, the bunch will shear into the shape of the tilted capital letter 'N', as shown by simulation in the right plot of Fig. 8. This is, in fact, a potential-well distortion of the rf wave, and can be cured, to a certain extent, by having rf systems of high frequencies, (see Sec. III B below).

III MICROWAVE INSTABILITY NEAR TRANSITION

A Analytic Solutions

In an operation near the transition energy ($\eta_0 \approx 0$), at least the next order, η_1 in Eq. (2.1), must be included for a meaningful discussion of the beam dynamics. Bogacz analyzed the stability of a coasting beam right at transition, $\eta_0 = 0$ [3], by including the η_1 term but neglecting other higher-order terms. For a Gaussian distribution with rms energy spread σ_E, he obtained an analytic expression for the growth rate at the revolution harmonic n:

$$\frac{1}{\tau_n} = -2\alpha_1 n\omega_0 \left(\frac{\sigma_E}{E_0}\right)^2 \phi_n \qquad \text{with} \qquad \tan\phi_n = \left[\frac{\mathcal{I}m\, Z_0^{\|}}{\mathcal{R}e\, Z_0^{\|}}\right]_n , \tag{3.5}$$

where $\mathcal{I}m\, Z_0^{\|} > 0$ implies capacitive and $\omega_0/(2\pi)$ is the revolution frequency of the on-energy particle which has energy E_0. He drew the conclusion that the beam will be completely stable. However, when he made this conclusion, he had in mind the assumption of $\alpha_1 > 0$ and $\phi_n > 0$, which is not always true. As a result, there will be microwave growth in general.

Holt and Colestock studied the same problem with coasting beam and Gaussian energy distribution, but allowing $\eta_0 \neq 0$ [4]. The dispersion relation is expressed in terms of the complex error function. Their conclusion is that there is no unstable region in the complex $Z_0^{\|}$-plane below transition. On the other hand, there are both stable and unstable regions above transition. They also claimed that their conclusion was supported by simulations. However, they did not specify the values of η_0 and η_1 in the simulations they presented or in their stability plots in the complex $Z_0^{\|}$-plane. It is hard to understand at least the situation below transition. It is clear that when $|\eta_0|$ is not too small, the contribution of η_1 is irrelevant. Thus their claim as stated can be interpreted as *no microwave instability below transition*, no matter how far away it is from transition. For this reason, this claim is quite questionable.

When we look into the stability plots of Holt and Colestock, we can see something that resembles a stability curve below transition, although the stability plots have been poorly drawn and are almost illegible. The presence of a stability curve implies the existence of both stable and unstable regions, in contradiction to their conclusion. We performed some simulations and have different results. We consider a coasting beam at 100 GeV in a hypothetic ring of circumference 50 m, with a rms parabolic fractional momentum spread of 0.001, interacting with a broadband impedance of $Z_0^{\|}/n = 3.00\ \Omega$ at the resonance frequency of 600 MHz and quality

factor $Q = 1$. This small size of ring is chosen because we want to limit the number of longitudinal bins around the ring so that not so many macro-particle will be necessary. The Keil-Schnell circle-approximated criterion gives a limit of $|Z_0^{\|}/n| = 1.00\ \Omega$ [5]. The results are shown in Fig. 9: the top 4 plots for $\eta = -0.005$ (below transition) and the lower 4 plots for $\eta = +0.005$ (above transition) at 0, 1200, 2400, and 3600 turns. We see that below transition irregularities develop at the low-momentum edge and the momentum spread broadens at the low-momentum side until the total spread is about 1100 MeV, about 2.75 times from the original total spread of about 400 MeV. This definitely confirms the occurrence of microwave instability below transition, and the eventual self-stabilization by overshooting. Above transition, irregularities also develop at the low-momentum edge and the momentum spread also broadens at the low-momentum edge. The total spread appears to be broader than the situation below transition. In addition, we see small bomb-like droplets launched at the low-momentum side, which is not observed below transition. We will come back to the simulations of coasting beam near transition later in Sec. III C.

B Bunched Beam Simulations

In this section, we study the stability of a bunched beam very close to transition. As an example, take a muon bunch in the proposed 50×50 GeV muon collider, which has a slip factor of $|\eta| = 1 \times 10^{-6}$. Everything we discuss here will apply to a proton bunch also, with the exception that the muons decay while the protons are stable. We will first discuss the situation with the decay of the muons taken into consideration, and later push the lifetime to infinity. We assume that sextupoles and octupoles are installed and adjusted so that the contributions of η_1 and η_2 become insignificant compared with η_0. The muon bunch we consider has an intensity of $N_b = 4 \times 10^{12}$ particles, rms width $\sigma_\ell = 13$ cm and rms fractional momentum spread $\sigma_\delta = 3 \times 10^{-5}$ or $\sigma_E = 1.5$ MeV. The impedance is assumed to be broadband with $Z_0^{\|}/n = 0.5\ \Omega$ at the angular resonant frequency of $\omega_r = 50$ GHz with quality factor $Q = 1$. The muons have an e-folding lifetime of 891 turns at 50 GeV in this collider ring. During the muon lifetime, there is negligible phase motion. Thus a bunching rf frequency system is not necessary. However, as will be explained below, rf systems are needed for the cancellation of potential-well distortion.

For bunched beams, there is the issue of potential-well distortion which must not be mixed up with the collective microwave instability. Potential-well distortion will change the shape of the bunch to something that looks like the right plot of Fig. 8, with the difference that the distortion of the beam does not come from the space-charge force, but mainly from the inductive part of the broadband impedance. The wake potential seen by a particle inside a Gaussian bunch at a distance z behind the bunch center is shown in the left plot of Fig. 10 and is given by

$$V(z) = e\int_{-\infty}^{z} dz'\rho(z')W_0(z-z') = -\frac{eN\omega_r R_{\|}}{2Q\cos\phi_0}\,\mathcal{R}e\, e^{j\phi_0 - z^2/(2\sigma_\ell^2)} w\left[\frac{\sigma_\ell\omega_r e^{j\phi_0}}{c\sqrt{2}} - \frac{jz}{\sqrt{2}\sigma_\ell}\right],$$

where $\rho(z)$ is the bunch distribution, $W_0(z)$ the longitudinal wake function, $\sin\phi_0 =$

$1/(2Q)$, and w is the complex error function. This distortion can be cancelled up to $\pm 3\sigma_\ell$ by 2 rf systems [6], which at injection are at frequencies $\omega_1/(2\pi) = 0.3854$ GHz and $\omega_2/(2\pi) = 0.7966$ GHz, with voltages $V_1 = 65.40$ kV and $V_2 = 24.74$ kV, and phases $\varphi_1 = 177.20°$ and $\varphi_2 = 174.28°$. This compensation is shown in the left plot of Fig. 10. Since only 2 sinusoidal rf's are used, the cancellation is not complete; however, the error is less than 1% of the original wake potential and is not important. Because of the lifetime of the muons, we first performed tracking for only 1000 turns in the time domain using the broadband wake function $W_0(z)$. The initial and final bunch distributions are shown in Fig. 11. During the simulation the

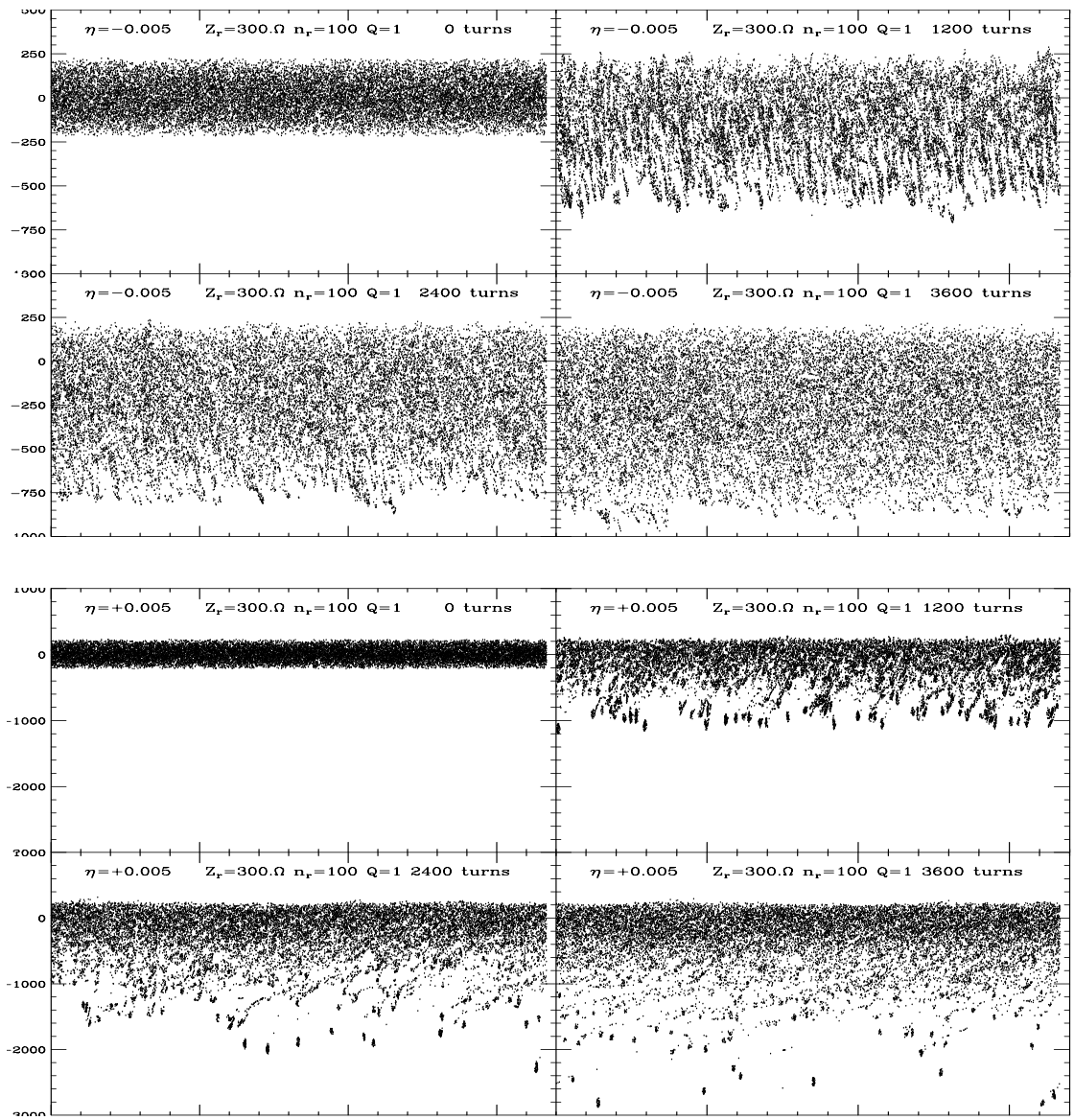

FIGURE 9. The top 4 plots and lower 4 plots are for $\eta = -0.005$ (below transition) and $\eta = +0.005$ (above transition), respectively, at 0, 12000, 24000, and 36000 turns. The impedance is a broadband with $Q = 1$, $Z_0^{\parallel}/n = 3.0\ \Omega$ at the resonant frequency of 600 MHz.

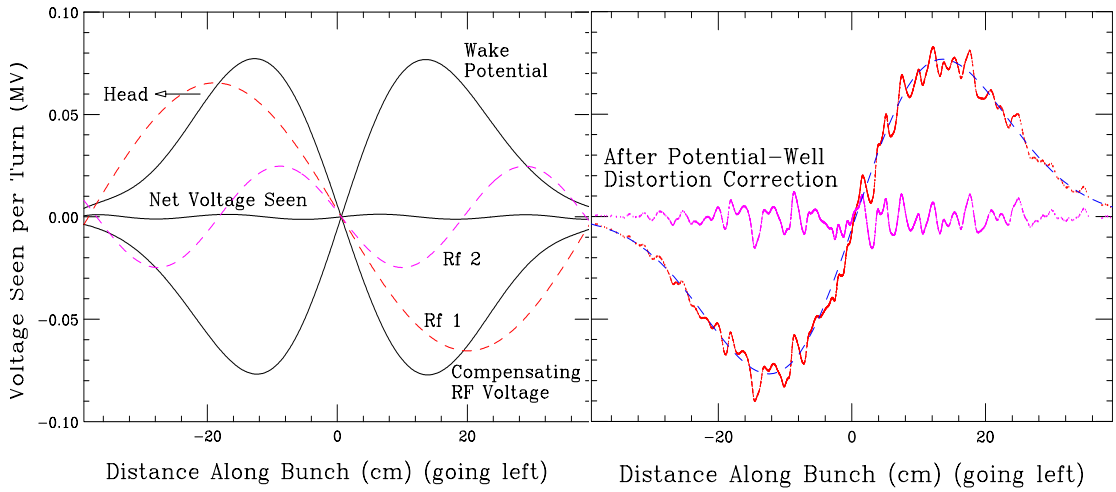

FIGURE 10. Left: Wake potential, compensating rf voltages, and net voltage seen by particles in the 13-cm bunch at injection. The compensating rf is the sum of two rf's represented by dashes. Right: Wake potential seen by the simulated bunch shown as dots is interlaced with the wake potential of an ideal smooth Gaussian bunch shown in dashes. The difference (center curve) represents the random fluctuation of the finite number of macro-particles.

compensating rf voltages were lowered turn by turn to conform with the diminishing bunch intensity due to the decay of the muons.

We see from the right plot of Fig. 11 that the bunch distribution has been very much distorted after 1000 turns. This comes mostly from the fact that the original distribution of the bunch in the left plot is not exactly Gaussian. It consists of 2×10^6 macro-particles randomly distributed according to a bi-Gaussian distribution. As a result, the wake potential of the actual bunch shown as a dotted curve in the right plot of Fig. 10 deviates slightly from and wiggles around the ideal wake potential curve of a smooth Gaussian bunch shown in dashes. The difference is the dotted jitter curve in the center of the plot. The fluctuation seen in the right plot of Fig. 11 is the result of the accumulation of this dotted jitter curve in 1000 turns with muon decay taken into account. Although this tiny fluctuation leads to a small potential-well distortion in one turn (≤ 0.02 MeV), it is unfortunate that it will accumulate turn after turn and will never reach a steady state, since the beam is so close to transition. This accumulated distortion can be computed exactly from the the dotted jitter curve. Any growth in excess will come from collective microwave instability. Note that the uncompensated potential-well distortion is quite different from the growth due to microwave instability. For the former, the growth in energy fluctuations every turn will be exactly by the *same* amount as given by the dotted jitter curve in the right Fig. 10 (if muon decay is neglected). This is because the wake potential of particles along the bunch does not depend on the energy distribution of the bunch, but only on its linear density and the latter is essentially unchanged since the particles do not drift much during the first 1000 turns. On the other hand, the initial growth due to microwave instability at a particular turn is proportional to the actual energy fluctuation at that turn

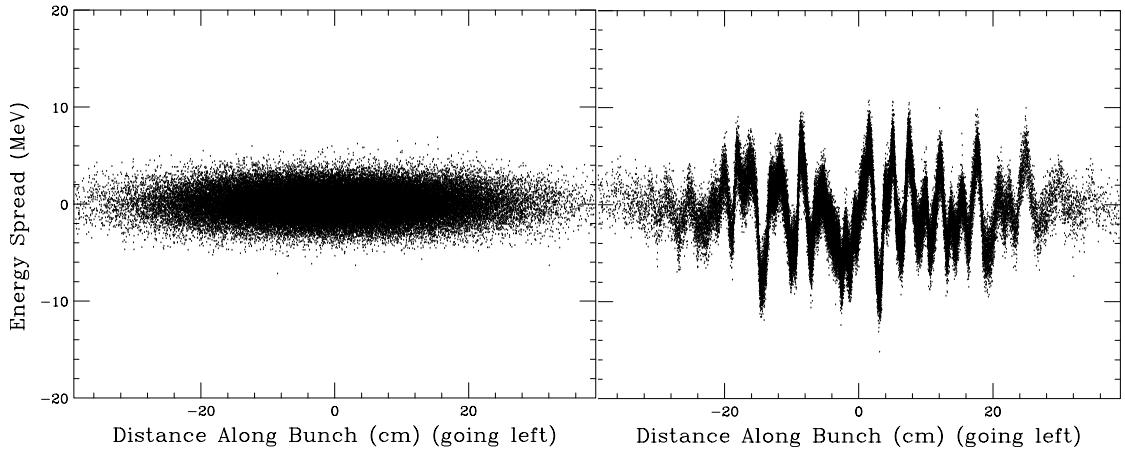

FIGURE 11. Simulation of the 13-cm bunch of 4×10^{12} muons subject to a broad-band impedance with quality factor $Q=1$ and $Z_{\parallel}/n=0.5\ \Omega$ at the resonant angular frequency $\omega_r=50$ GHz. The half-triangular bin width is 15 ps (0.45 cm) and 2×10^6 macro-particles are used. Left plot shows initial distribution with $\sigma_E=1.5$ MeV and $\sigma_\ell=13$ cm. Right plot shows distribution after 1000 turns with compensating rf's depicted in Fig. 10.

and the evolution of the growth is exponential. Thus, although the growth due to microwave instability is small at the beginning, it will be much faster later on when the accumulated energy fluctuations become larger. It is worth mentioning that even if the wake potential of the initial bunch with statistical fluctuations has been compensated exactly by the rf's, the bunch can still be unstable against microwave instability. An infinitesimal deviation from the bunch distribution can excite the collective modes of instability corresponding to some eigenfrequencies. In other words, the accumulated growth due to potential-well distortion is a static solution and this static solution converges very slowly close to transition until the momentum spread is large enough for the small $|\eta|$ to smooth the distribution. Microwave instability, on the other hand, is a time dependent solution.

In Fig. 12, the 3 plots on the left are for a 4000-turn simulation of the same muon bunch using 2×10^6 macro-particles with the decay of the muons considered. The two compensating rf systems are turned on. The first plot is for $\eta = 0$ so that microwave instability cannot develop. All the fluctuations are due to the residual potential-well distortion or the accumulation of the uncompensated jitters. The second and third plots are for, respectively, $\eta = -1 \times 10^{-6}$ (below transition) and $\eta = +1 \times 10^{-6}$ (above transition). We see that they deviate from the first plot, showing that there are growths due to microwave instability although the effect is small. The 3 plots on the right are the same as on the left with the exception that the muons are considered stable, or, in other words, the particles can be protons. We see that the second and third plots differ from the first one by very much (note the change in energy scale), indicating that microwave instability does play an important role for proton bunches in a quasi-isochronous ring. We also see that microwave instability is more severe above transition than below transition even when the beam is so close to transition.

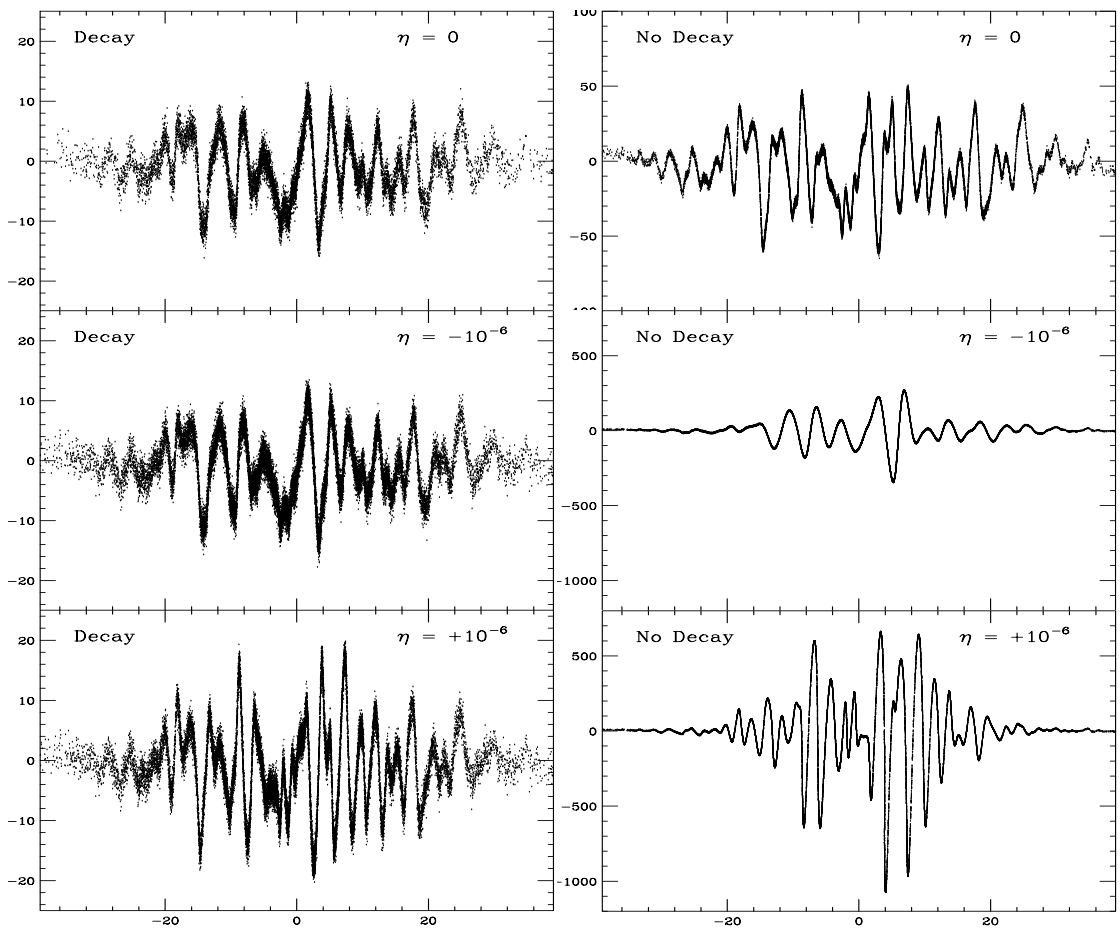

FIGURE 12. Phase-space plots of energy spread in MeV versus distance from bunch center in cm at the end of 4000 turns. All are simulating 4×10^{14} micro-particles with 2×10^{6} macro-particles. In the left 3 plots, the decay of the muons has been taken into account. The first left plot is for $\eta = 0$ so that it just gives the amount of potential-well distortion. The second and third plots are for, respectively, $\eta = -1 \times 10^{-6}$ and $+1 \times 10^{-6}$. The small deviations from the first plot are results of microwave instability. The right 3 plots are the same as the left, except that the muons are considered stable. Here, large microwave growths develop (note the change of energy scale).

C Coasting Beam Simulations

For coasting beams, we do not have the inverted tilted "N"-shape wake potential as in Fig. 10. Thus, no rf compensation will be required. However, the noise in the beam does result in a wake potential similar to the small residual wake-potential jitters in Fig. 10 after the rf compensation. Near transition where the phase motion is negligibly slow, these jitters will add up turn after turn without limit exactly in the same way as the bunched beam after having optimized the rf compensation. Thus, near transition, there is essentially no difference between a coasting beam and a bunched beam after the rf compensation. The only exception is that microwave instability develops most rapidly near the center of the bunch where the local intensity is highest, whereas in a coasting beam, microwave instability develops

with equal probability along the bunch depending on the statistical fluctuations in the macro-particles.

In Fig. 13, we show some coasting beam simulations near transition by having $\eta_0 = 0$ or $\pm 5 \times 10^{-5}$ and $\eta_1 = 0$ or ± 0.05. The coasting beam consists of 3.27×10^{15} protons (or nondecaying muons) having an average energy of 100 GeV in a hypothetic ring with circumference 50 m. The initial momentum spread is Gaussian with rms fractional spread $\sigma_\delta = 0.001$ or $\sigma_E = 100$ MeV. Thus, at 1σ, the contribution of $|\eta_1| = 0.05$ is the same as the contribution of $|\eta_0| = 5 \times 10^{-5}$. The simulations are performed with 8×10^5 macro-particles in 400 triangular bins. The impedance is a broadband with $Q = 1$ and $Z_0^{\|}/n = 2\ \Omega$ at the resonant frequency of $f_r = 300$ MHz.

All the plots in Fig 13 are illustrated with the same scale for easy comparison. The horizontal axes are longitudinal beam position from 0 to 166.7 ns, while the vertical axes are energy spread from -4000 to 3000 MeV. Plot (a) shows the initial particle distribution in the longitudinal phase space. All the other plots are simulation results at the end of 54,000 turns. Plot (b) is the result of having $\eta_0 = 0$ and $\eta_1 = 0$. It shows the accumulation of the wake-potential jitters over 54,000 turns. These jitters originate from the statistical fluctuation of the initial population of the macro-particles. Therefore, any deviation from Plot (b) implies microwave instability. Plots (c) and (d) are with $\eta_0 = 0$, but with $\eta_1 = +0.05$ and -0.05, respectively. We see the growths curl towards opposite phase directions nonlinearly as expected. This is due to the nonlinearity in δ in the time slip given by Eq. (2.4), similar to the simulations in Fig. 8(a). It appears that Plot (c) with $\eta_1 = -0.05$ gives a larger growth. Plots (e), (g), and (i) are for $\eta_0 = -5 \times 10^{-5}$ (below transition), but with $\eta_1 = +0.05$, -0.05, and 0, respectively. We see that the microwave instability is most severe when $\eta_1 = 0$, indicating that η_1 has the ability to curb instability. This is, in fact, easy to understand. The phase drift driven by $|\eta_1| = 0.05$ is much faster than that driven by $|\eta_0| = 5.0 \times 10^{-5}$ at larger momentum spread; for example, it will be 4 times faster at $2\sigma_\delta$, 9 times faster at $3\sigma_\delta$, etc. As a result, a nonvanishing $|\eta_1|$ tends to move particles away from the clumps, thus lessening the growth due to microwave instability.

Plots (f), (h), and (j) are for $\eta_0 = +5 \times 10^{-5}$ (above transition), but with $\eta_1 = +0.05$, -0.05, and 0, respectively. Again microwave instability is most severe when $\eta_1 = 0$, and η_1 does curb instability to a certain extent. Comparing Plots (e), (g), and (i) with Plots (f), (h), and (j), it is evident that the beam is more unstable against microwave instability above transition ($\eta_0 > 0$) than below transition ($\eta_0 < 0$) independent of the sign of η_1. For a fixed η_0, we also notice that negative η_1 is more unstable than positive η_1. The theoretical implications of these results are nontrivial and will be discussed in a future publication.

Now let us come back to the analytic investigations by Bogacz, Holt, and Colestock. Their results appear to contradict the simulations presented here. Analytic analysis often starts with the Vlasov equation. The time-dependent beam distri-

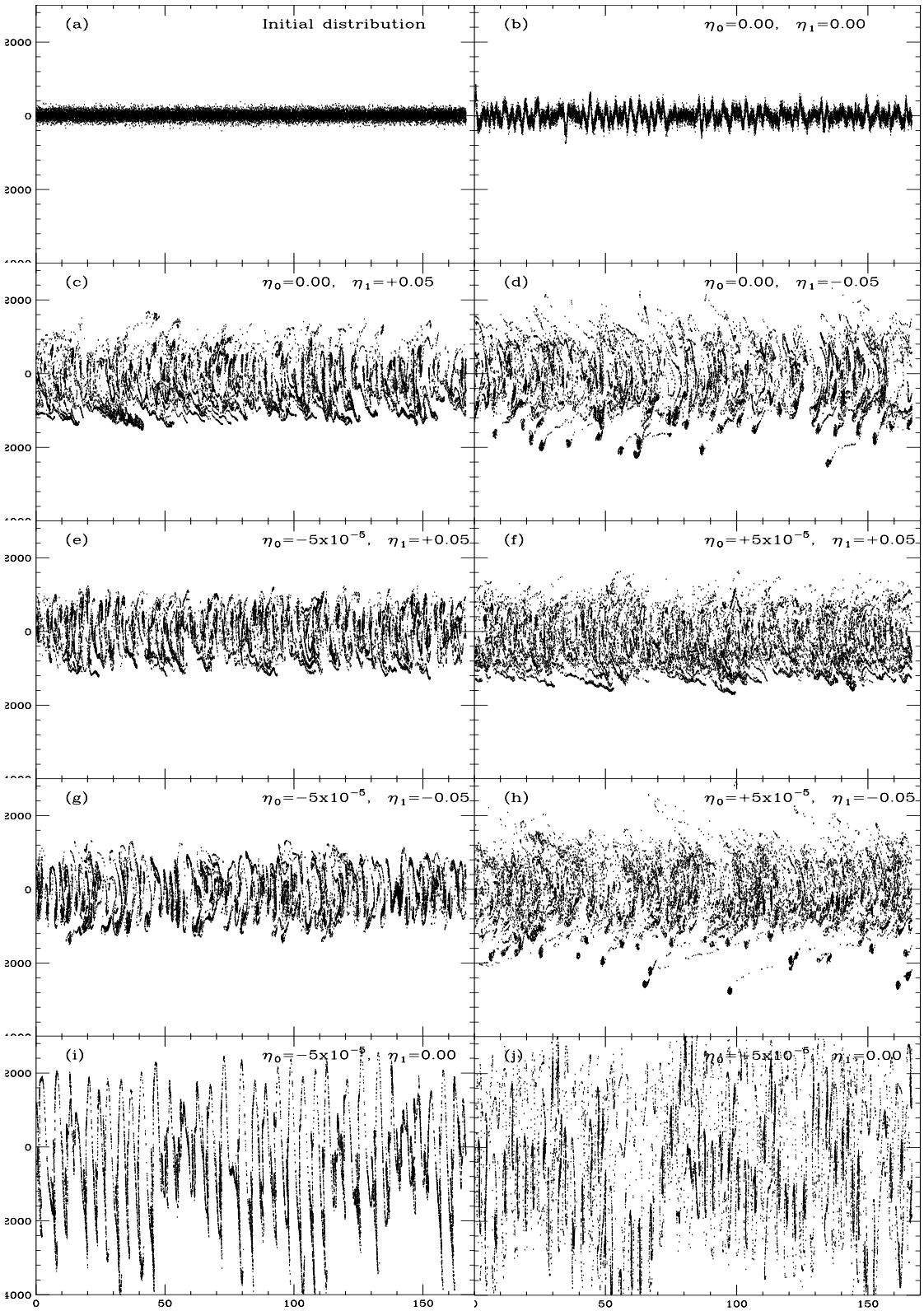

FIGURE 13. Energy spread (MeV) versus bunch position (ns) of coasting beam simulations. See text for explanation.

bution $\psi(\phi, \Delta E; t)$ can be separated into two parts:

$$\psi(\phi, \Delta E; t) = \psi_0(\phi, \Delta E) + \psi_1(\phi, \Delta E)e^{-i\Omega t} \ . \tag{3.6}$$

Here, ψ_0 is the *steady-state* solution of the Hamiltonian and ψ_1 describes the collective motion of the beam with the collective frequency $\Omega/(2\pi)$. After linearization, the Vlasov equation becomes an eigenequation with ψ_1 as the eigenfunction and $\Omega/(2\pi)$ the eigenfrequency. The equation also depends on ψ_0. Thus we must solve for the *steady-state* solution first before solving the eigenequation. The steady-state solution is the time-independent solution of the Hamiltonian which includes the contribution of the wake function. In other words, ψ_0 is the potential-well-distorted solution. Far away from transition, this distortion is mostly in the ϕ coordinate, for example, those brought about by the space-charge or inductive forces. Therefore, for a coasting beam, there will not be any potential-well distortion at all. The situation, however, is quite different close to transition. As was pointed out in above, the potential-well distortion is now in the ΔE coordinate. For this reason, not only bunched beams, even coasting beams will suffer from potential-well distortion as a result of the nonuniformity of the beam. In simulations, the nonuniformity arrives from the statistical fluctuation of the distribution of the macro-particles. This nonuniformity will accumulate turn by turn until the momentum spread is so large that the small $|\eta|$ is able to smooth out all nonuniformity. In other words, the steady-state distribution ψ_0 that goes into the Vlasov equation will be completely different from the original distribution in the absence of the wake. In the analysis of Bogacz, Holt, and Colestock, the ideal smooth Gaussian distribution in energy was substituted for ψ_0 in the Vlasov equation. However, this is a very unstable static distribution; even a small perturbation will accumulate turn by turn with extremely slow convergence. For this reason, it is hard to understand what their results really represent.

REFERENCES

1. Trbojevic, D.,Brennan, J.M., Courant, E.D., Roser, T., Peggs, S., Ng, K.Y., Johnstone, C., Popovic, M., Norem, J., *A Proton Driver for the Muon Collider Source with a Tunable Momentum Compaction lattice*, *Proceedings of IEEE Particle Accelerator Conference*, p.1030 (Vancouver, Canada, 1997).
2. Ankenbrandt, C, Ng, K.Y., Norem, J., Popovic, M., Qian, Z., Ahrens, L.A., Brennan, M., Mane, V., Roser, T., Trbojevic, D., and van Asselt, W., *Phys. Rev. ST Accel. Beams*, **1**, 030101 (1999).
3. Bogacz, A.S., *Microwave Instability at Transition—Stability Diagram Approach*, *Proceedings of IEEE Particle Accelerator Conference*, p.1815 (San Francisco, CA, 1991).
4. Holt, J.A, and Colestock, P.I., *Microwave Instability at Transition*, *Proceedings of IEEE Particle Accelerator Conference*, p.3067 (Dallas, TX, 1995).
5. Keil, E., and Schnell, W., CERN Report TH-RF/69-48, 1969.
6. Kim, E.-S., Sessler, A.M., and Wurtele, J.S., *Phys. Rev. ST Accel. Beams*, **2**, 051001 (1999).
7. Ng, K.Y., *Phys. Rev. ST Accel. Beams*, **2**, 091001 (1999).